Experimental and Molecular Pathology 125 (2022) 104759

Contents lists available at ScienceDirect

Experimental and Molecular Pathology

journal homepage: www.elsevier.com/locate/yexmp

Laser desorption tissue imaging with Differential Mobility Spectrometry

Maiju Lepomäki [a,d,*], Anna Anttalainen [b,c], Artturi Vuorinen [c], Teemu Tolonen [d], Anton Kontunen [b,c], Markus Karjalainen [b,c], Antti Vehkaoja [c], Antti Roine [a,b], Niku Oksala [a,b,e]

[a] Surgery, Faculty of Medicine and Health Technology, Tampere University, Kauppi Campus, Arvo Building, Arvo Ylpön katu 34, 33520 Tampere, Finland
[b] Olfactomics Ltd, Kampusareena, Korkeakoulunkatu 7, FI-33720 Tampere, Finland
[c] Sensor Technology and Biomeasurements, Faculty of Medicine and Health Technology, Tampere University, Hervanta Campus, Sähkötalo Building, Korkeakoulunkatu 3, FI-33720 Tampere, Finland
[d] Department of Pathology, Fimlab Laboratories, Arvo Ylpön katu 4, FI-33520 Tampere, Finland
[e] Vascular Centre, Tampere University Hospital, Central Hospital, P.O. Box 2000, FI-33521 Tampere, Finland

ARTICLE INFO

Keywords:
Differential Mobility Spectrometry (DMS)
Field asymmetric ion mobility spectrometry (FAIMS)
Tissue imaging
Tissue mapping
Breast cancer

ABSTRACT

Pathological gross examination of breast carcinoma samples is sometimes laborious. A tissue pre-mapping method could indicate neoplastic areas to the pathologist and enable focused sampling. Differential Mobility Spectrometry (DMS) is a rapid and affordable technology for complex gas mixture analysis. We present an automated tissue laser analysis system for imaging approaches (iATLAS), which utilizes a computer-controlled laser evaporator unit coupled with a DMS gas analyzer. The system is demonstrated in the classification of porcine tissue samples and three human breast carcinomas. Tissue samples from eighteen landrace pigs were classified with the system based on a pre-designed matrix (spatial resolution 1–3 mm). The smoke samples were analyzed with DMS, and tissue classification was performed with several machine learning approaches. Porcine skeletal muscle ($n = 1030$), adipose tissue ($n = 1329$), normal breast tissue ($n = 258$), bone ($n = 680$), and liver ($n = 264$) were identified with 86% cross-validation (CV) accuracy with a convolutional neural network (CNN) model. Further, a panel tissue that comprised all five tissue types was applied as an independent validation dataset. In this test, 82% classification accuracy with CNN was achieved. An analogous procedure was applied to demonstrate the feasibility of iATLAS in breast cancer imaging according to 1) macroscopically and 2) microscopically annotated data with 10-fold CV and SVM (radial kernel). We reached a classification accuracy of 94%, specificity of 94%, and sensitivity of 93% with the macroscopically annotated data from three breast cancer specimens. The microscopic annotation was applicable to two specimens. For the first specimen, the classification accuracy was 84% (specificity 88% and sensitivity 77%). For the second, the classification accuracy was 72% (specificity 88% and sensitivity 24%). This study presents a promising method for automated tissue imaging in an animal model and lays foundation for breast cancer imaging.

1. Introduction

Alternatives to traditional microscopy for the examination of tissues for malignancy have recently captured attention in the field of diagnostics and surgical treatment of breast cancer. The evaluation of surgical margins after breast-conserving surgery (BCS) is of special interest as positive margins remain a problem (Senkus et al., 2015; Cardoso et al., 2019). The rate of reoperations due to margin positivity in BCS is relatively high at approximately 30% (Lovrics et al., 2009; van Leeuwen et al., 2018). This has motivated the development of several tools for margin assessment that utilize different technical approaches. To suit clinical practice, the method should be fast, offer high spatial resolution, and a sensitivity approaching 95% to minimize the risk of false negatives (Maloney et al., 2018).

The histopathological analysis of breast cancer aims to determine the tumor type and grade; surgical margin status; and pathological stage

Abbreviations: BCS, Breast-conserving surgery; VOC, Volatile organic compound; DMS, Differential Mobility Spectrometry; FAIMS, Field asymmetric ion mobility spectrometry; MSI, Mass spectrometry imaging; MS, Mass spectrometry; iATLAS, Automated tissue laser analysis system; TAUH, Tampere University Hospital; H&E, Hematoxylin and Eosin; CV, Cross-validation; sLDA, Shrinkage linear discriminant analysis; SVM, Support vector machine; CNN, Convolutional neural network; MALDI, Matrix assisted laser desorption/ionization; DESI, Desorption electrospray ionization; REIMS, Rapid evaporative ionization mass spectrometry.

* Corresponding author at: Tampere University, Kauppi campus, Arvo Building, Arvo Ylpön katu 34, 33520 Tampere, Finland.
E-mail address: maiju.sutinen@tuni.fi (M. Lepomäki).

https://doi.org/10.1016/j.yexmp.2022.104759
Received 8 September 2021; Received in revised form 27 February 2022; Accepted 19 March 2022
Available online 23 March 2022

(pTNM stage). During gross examination of the breast, the specimen is first sliced to 5–10 mm sections, which are then visually examined and palpated. Based on the findings on grossing, representative samples are taken from the areas that most likely contain malignant tissue; the smallest surgical margins; mamillary region if included in the resection; and all breast quadrants (random blocks). The entire specimen is seldom processed for histological analysis (Morrow, 2009). In many instances the grossing is straightforward. However, sometimes the examination poses a challenge to the pathologist. On palpation, the consistency of malignant tumors tends to be harder as opposed to benign areas, but this feature is not solely reliable. Also, the visual distinction between benign fibrous tissue, *in situ* carcinoma, and invasive carcinoma can be impossible in cases with concurrent mastopathy or after neoadjuvant treatment. Tumor multifocality and lobular subtype highlight these problems. The sensitivity of gross intraoperative margin assessment for breast cancer has been shown defective at 49%. Multifocality on final pathology was associated with a false negative intraoperative assessment (Nunez et al., 2020). When pathologists are uncertain, they are prone to take more samples, yielding to an increased workload for both the laboratory and pathologists. A sensitive tissue imaging method could aid pathologists by indicating neoplastic areas before or during the gross examination and thus enable better-focused sampling. Tissue imaging could also benefit staging in the determination of tumor size and be practical in the sampling of the surgical margin to ensure complete cancer removal. In addition, tissue imaging could enable a reduced number of blocks analyzed per specimen without compromising diagnostic accuracy. POIS: (Balog et al., 2013; St John et al., 2017).

The molecular differences between benign and cancerous breast tissues stem from their distinct lipid phenotypes and metabolic features. Cancer cells rewire their metabolism to promote cancer cell survival, proliferation, migration, invasion, metastasis, and suppression of antitumor responses. The distinguishing features of this phenomenon, also known as “The Warburg effect”, are increased glucose uptake and fermentation of glucose to lactate (Liberti and Locasale, 2016; Vaupel et al., 2019). In addition to changes in glucose metabolism, tumors undergo lipid metabolic abnormalities such as increased fatty acid oxidation and *de novo* lipid synthesis (Corna et al., 2020). Altogether, these metabolic changes are reflected in the Volatile organic compound (VOC) profiles of evaporated tissues and allow for the distinction of breast cancer from surgical smoke (Balog et al., 2013; St John et al., 2017). Breast cancer has been shown to display increased levels of fatty acids and glycerophospholipids as opposed to normal breast tissues (St John et al., 2017; Guenther et al., 2019). In addition, tumor associated stroma clearly separated from the stromal tissue beyond the surgical resection margin, highlighting the fact that stromal tissue within the tumor microenvironment also undergoes detectable metabolic changes (Guenther et al., 2019).

Differential Mobility Spectrometry (DMS), also known as Field Asymmetric Ion Mobility Spectrometry (FAIMS), enables the analysis of complex gas mixtures. In DMS, gaseous molecules are ionized and conducted to a strong, altering electric field. The trajectories of the molecules differ according to their shape, size and charge which consequents to their separation. The molecular composition of the sample is presented as a dispersion plot, which provides a data-rich chemical fingerprint of the sample (Covington et al., 2015; Cumeras et al., 2015). DMS has been studied in several medical applications (Covington et al., 2015); applied as a prefilter for mass spectrometry (MS) in the analysis of complex lipid mixtures (Shvartsburg et al., 2011; Hancock et al., 2019); and independently in the estimation of lipid concentrations (Anttalainen et al., 2021). Its core advantages are the omission of vacuum and good intra-device stability after initial validation.

Mass spectrometry imaging (MSI) techniques enable rapid molecular diagnostics of tissues. MSI has been demonstrated in the visualization of human liver samples with metastases (Golf et al., 2015) and colorectal cancer (Veselkov et al., 2014; Mirnezami et al., 2014). MS approaches have also been successfully applied in the molecular imaging of breast cancer (Guenther et al., 2015; St John et al., 2017; Zhang et al., 2017). Although MSI techniques are efficient, they are complex, time-consuming and financially straining which limit their feasibility outside research facilities. Tissue imaging with DMS provides a less complex and more economical alternative to MSI while retaining the ability to qualitatively assess the molecular composition of the tissue.

We have previously presented a novel DMS system for breast and brain tumor identification from surgical smoke (Sutinen et al., 2019; Haapala et al., 2019) and explored DMS feasibility in tissue imaging with porcine tissues (Kontunen et al., 2020). In these studies, we have coupled DMS with a diathermic knife. However, former MS studies have also utilized CO_2 laser data in tissue identification with improved spectral quality and good reproducibility as opposed to electrocautery (Sächfer et al., 2011; Genangeli et al., 2019). The advantage of laser sampling is the possibility to analyze non-conductive hard tissues such as bone (Genangeli et al., 2019). Precise laser analysis can be performed even on thin tissue sections along with the energy adjusted as appropriate (Ogrinc et al., 2019). A diathermic knife creates soot during incision, which can lead to the cross-contamination of consecutive measurements, whereas a laser is positioned far from the sample to reduce carry-over.

In this article, we present an automated tissue laser analysis system for imaging approaches (iATLAS), which utilizes a DMS device coupled with a laser evaporation unit. In addition, we introduce a comprehensive set of methods suitable for the analysis of DMS data. First, the operating principle is demonstrated in porcine tissues. Second, we explore the feasibility of iATLAS in human breast cancer imaging. The goal of the study is to present an efficient method for tissue imaging with minimal sample preparation.

2. Material and methods

2.1. Measurement system and sampling protocol

iATLAS comprised a sampling stage; a K40-type computer numerical control (CNC) laser cutter (CO_2 Laser engraving machine, BeautyDirectMall, China), which was enhanced by improved computer-controlled stepper motor drivers; a gas sample pre-processing unit; and an ENVI-AMC® DMS device (Environics Oy, Mikkeli, Finland). The pre-processing unit and the DMS device have previously been described in detail by Kontunen et al. (Kontunen et al., 2018) A schematic illustration of the measurement system is presented in Fig. 1.

The laser source was a 40 W 10,600 nm CO_2 -laser which was factory-installed in the K40 CNC machine. The laser was chosen for its easy modification and affordability. Its control electronics and software were replaced with custom ones. The laser cutter was equipped with a sample platform to facilitate easy sample height adjustment and device clean up. The optical path of the laser consisted of a fixed laser tube and moving gantry, which held the collimation lens and smoke sampling nozzle assembly. The nozzle assembly comprised a smoke sample port and an annular purge air nozzle to keep room air impurities out from the smoke sample. Filtered compressed air, bubbled through water, maintained consistent moisture.

Each specimen was analyzed in an automated measurement sequence. A 2 ms pulsed laser measurement was repeated 300 times during a 30 s time period. The laser pulsation was kept constant to stabilize the concentration of smoke. After laser evaporation, the smoke sample passed through a pre-processing unit employing a corona discharge filter to remove particle impurities that could contaminate the DMS sensor. The duration of analysis was 22 s, after which the system cleaned itself with purified air for 50 s to prevent carry-over.

For each measurement point, the DMS analyzer was set to produce a 480-point DMS data matrix for positive ions, which represented the ion spectrum of the smoke sample. The intensity values that formed the dispersion matrix were 40 U_{cv} values from - 2.4 kV/m to 20 kV/m and 48 kV/m U_{sv} values from 1400 kV/m to 2800 kV/m.

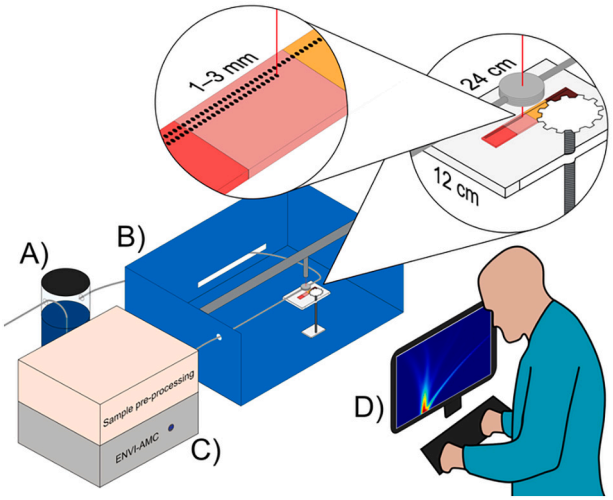

Fig. 1. A schematic illustration of the measurement system. The system consists of: A) Air humidifier for the carrier gas; B) Sampling platform; C) DMS sensor; and D) Graphical user interface. The entire system is controlled by the user interface, which communicates with the other components *via* an Ethernet connection. The laser is used to generate a gaseous sample from the tissue, which is collected by the sampling nozzle, and filtered in the sample conditioner. After filtration, the sample is analyzed with the DMS system, and the results are automatically stored in a web database. The sampling nozzle is equipped with buffer air to keep contamination out of the sample.

2.2. Study materials

The animal tissues included in the study were gathered from eighteen Finnish landrace pigs (*Sus scrofa domesticus*) between October 2019 and March 2020. The surgical specimens of breast cancer were gathered from three breast cancer patients that were operated on at Tampere University Hospital (TAUH) between December 2019 and January 2020. The porcine tissues were commercial slaughterhouse products from livestock animals and comprised adipose tissue, skeletal muscle, breast tissue, liver, and bone tissue (vertebra). The preparation of animal samples was performed by a medical doctor (M.L.). Breast cancer samples were collected by a breast pathologist (T.T.) at Fimlab Laboratories, which is the principal pathology laboratory in the TAUH region. This study has been approved by the Ethical Committee of TAUH (code R19059). No written patient consent was obtained because according to the Finnish Act on Medical Use of Human Organs, Tissues and Cells, anonymized specimens obtained for diagnostic purposes can be utilized in medical research with the permission of the organization handling the specimens (Institute of Biosciences and Medical Technology, 2017).

First, we conducted a series of measurements over a period of 13 days with homogenized porcine liver to assess the variance in environmental factors between measurement days. The porcine liver from one individual landrace pig was frozen fresh and homogenized with an immersion blender (ErgoMixx 600 W, BSH Hausgeräte GmbH, Germany). The homogenized liver samples were placed on Petri dishes and stored in a freezer (− 18 °C). The goal of tissue homogenization was to ensure alike samples in order to examine the effect of environmental factors on measurements rather than factors associated with the sample. Each day one sample was measured twelve times with a laser beam according to a pre-designed matrix (spatial resolution 2 mm) and the produced smoke was analyzed with DMS.

Second, we performed a large series of porcine tissue measurements. The prepared tissues (adipose, skeletal muscle, breast, liver, and bone tissue) were either analyzed immediately after preparation or stored frozen (− 18 °C) and analyzed after defrosting. In general, skeletal muscle, adipose, and non-homogenized liver tissue samples were analyzed as artificial mosaic panels comprising 2–4 individually dissected tissue types. This was not applicable to porcine breast tissue as the volume of breast parenchyma in each specimen was little. Therefore, the porcine breast tissue samples were analyzed as a part of a larger specimen (Sup. 3). Bone samples were primarily measured separately. In addition, a panel tissue comprising all five tissue types was analyzed for the matrix-wise tissue identification analysis. Finally, another panel of all five tissues was measured for the independent validation set analysis. The samples were placed in the sampling platform and three focusing points were measured to ease localization of measurements. Then, the specimen was analyzed according to a pre-designed matrix (spatial resolution 1–3 mm). All samples were photographed before and after sampling for subsequent annotation.

Third, an analogous procedure was applied to demonstrate the feasibility of iATLAS in breast cancer imaging in three carcinoma specimens. The inclusion criteria were 1) palpable tumor and 2) tumor size exceeding 20 mm (clinical tumor stage (cT) cT2 or above). The samples were gathered during the gross dissection of fresh surgical specimen, covered with a gauze moisturized with saline to prevent dehydration, stored at +4 °C and analyzed on the same day as the operation. After DMS sampling, the carcinoma specimens were fixated in formalin, stained with Hematoxylin and Eosin (H&E) and microscopically examined by a pathologist. The holes created by the laser to the first specimen were not visible on histopathological examination. Therefore, the laser measurements of the subsequent samples were reinforced with a 24 G cannula after sampling to ensure visibility after fixation and staining. The samples were annotated macroscopically from photographs similarly to the animal samples and microscopically according to their histopathological examination.

2.3. Classification models

Four different classification methods were employed in the classification of porcine tissue data: shrinkage linear discriminant analysis (sLDA); support vector machine (SVM) with linear and radial kernel; and convolutional neural networks (CNNs). sLDA has been shown successful in distinguishing porcine tissues from surgical smoke with DMS (Kontunen et al., 2018). However, it is possible that linear classifiers are not optimal in the separation of multidimensional DMS data. Thus, a relatively simple non-linear model was introduced with a radial kernel SVM and a more complex method with CNN. Data analysis was performed with the statistical software R (R Core Team, 2018). [sda] package was used for sLDA (Ahdesmaki et al., 2015); [e1071] for SVM (Meyer et al., 2019); and [keras] for R with TensorFlow in the backend for CNN (Abadi et al., 2016; Allaire and Chollet, 2019). For testing the daily variance, k-means clustering was performed with the [stats] package implementation (R Core Team, 2019).

LDA is a simple and effective method for data classification which utilizes dimensionality reduction techniques. This technique sets assumptions on data such as the normality assumption and uncorrelatedness of the data dimensions. In standard LDA, the number of training samples should be significantly higher than the number of original data dimensions, because otherwise the model formation is impaired. In these cases, regularization techniques ensure better results as they compensate the violation of data assumptions. For these reasons, we utilized a regularized version of the method, sLDA. A limitation of LDA and its regularized variants is that only linear separation of classes is enabled. (Ahdesmäki and Strimmer, 2010).

SVM is a machine learning method that aims to segregate classes within data by finding a hyperplane that best divides the dataset. If classes are linearly separable, linear SVM can be applied. However, real-life data is almost never linearly separable. In these cases, the so-called kernel trick can be applied to perform non-linear mapping to a new feature space, where linear separation is possible. Using soft margins allows misclassifications with overlapping classes and thus regularizes the model. In this study, we utilized both linear SVM and SVM with radial basis kernel function. The parameters controlling the soft margins

and the complexity of the model were optimized with internal cross-validation (CV) while training the models. (Cortes and Vapnik, 1995).

Artificial neural networks consist of computational units called neurons. These neurons are organized in consecutive layers that perform computational tasks on the input data and convey the result to the next layers. A neural network can be perceived as a nested structure of functions that eventually generate the target variable (*e.g.*, class label). CNNs have layers that enable feature extraction from image formats or two-dimensional (2D) data matrices, such as the dispersion matrices in this study. The classification results are formed from the extracted features of these layers. CNNs can model highly complex, non-linear phenomena. However, a high number of parameters need to be optimized when the model is formed. Despite their superior representative potential, they may perform deficiently if the training dataset is not vast (Goodfellow et al., 2016). The CNN used in this study is further described in the supplementary material (Sup. 1).

2.4. Data management

2.4.1. Porcine tissue samples

The porcine tissue dataset included 4245 smoke samples measured in forty-nine matrices. The daily measurements of homogenized liver were incorporated in this dataset. As previously described, the samples were visually annotated after analysis. The measurements located in the border region of two tissues ($n = 435$) were excluded from analysis as these could not be reliably annotated. Also, faulty dispersion plots due to sporadic malfunctions in the measurement device ($n = 64$) were excluded. The remaining dataset ($n = 3746$) was applied in the respective analyses 1) the assessment of daily variance utilizing the homogenized liver measurements ($n = 155$), 2) matrix-wise tissue identification ($n = 3561$), and 3) independent validation set analysis ($n = 185$). The intensities of dispersion plots were normalized to values from zero to one by scaling with matrix-wise minimum and maximum intensities. No other data pre-processing was performed.

To assess the daily variance, we examined the correlations between single measurements. The correlation was calculated as the Pearson's correlation between the intensity values of two measurements at the same locations of the dispersion matrices. In matrix-wise tissue identification and the independent validation set analysis, the performance of each classification models was estimated with leave-one-matrix-out CV. In leave-one-matrix-out CV, the data accumulated on one day performs as the testing dataset and the other groups as the training dataset. The process is repeated for all groups to achieve combined results. The matrix-wise tissue identification analysis assessed the suitability of each classification model to the analysis of DMS data. To showcase the classification of DMS data with an existing classification model, we performed the independent validation set analysis. We classified the latter analyzed panel tissue which comprised all five tissue types with the classification models constructed during the matrix-wise tissue identification analysis. The data of the validation set were not used in any part of the model training, selection, or hyper-parameter optimization processes.

2.4.2. Breast cancer specimens

The smoke samples included 499 measurements from three human breast cancer specimens. Three measurements were excluded due to device malfunction.

The measurements were macroscopically annotated according to photographs as benign or malignant ($n = 143$ and $n = 117$, respectively). The measurements that were in the border region and thus could not be reliably annotated, were categorized as uncertain ($n = 236$).

In two breast cancer specimens, we obtained the corresponding histology with distinguishable laser measurements. The measurement points were microscopically identified and annotated by a breast pathologist as benign or malignant ($n = 131$ and $n = 60$, respectively). The samples that contained only sporadic malignant cells were excluded as uncertain ($n = 63$) and the measurements that could not be identified from the histopathological image as missing (n = 60). Fig. 2 portrays the dimensions of the measurement points.

The number of smoke samples was few as this was a proof-of-concept study. To enable the analyses, we applied 10-fold CV and a SVM (radial kernel) classification model as the adequate training of CNN classifiers require large datasets. The reliably annotated measurements were randomly divided to ten equisized groups. Each group performed as the testing dataset at a time and the other nine groups as the training dataset, and the process was repeated for all ten groups. We report the combined results of all ten folds. To enable visualization of results, the 'uncertain' smoke samples were also classified with the trained model.

3. Results

3.1. Daily variation

The analysis included 155 porcine liver samples measured over 13 days. The result is presented as a correlation matrix (Sup. 2). The measurements that were analyzed on separate days correlated strongly. In comparison, the correlations between the first and the subsequent measurements of each sequence were weaker likely due to the warming up of the device during analysis. These findings support the generalizability of data as there were no significant differences between measurement days.

3.2. Porcine tissues

3.2.1. Matrix-wise tissue identification

The averaged dispersion matrices of each tissue type and their corresponding standard deviation matrices show visually distinguishable features (Fig. 3). The dataset comprised porcine skeletal muscle ($n = 1030$), adipose tissue ($n = 1329$), normal breast tissue ($n = 258$), bone tissue ($n = 680$), and liver ($n = 264$). The results obtained with the classification models are presented in Table 1. The classification accuracies ranged between 71% and 86%. The highest classification accuracy was reached with the CNN classifier. The specificity of the CNN classifier exceeded 90% for all tissue types. The highest sensitivity was reached for adipose tissue (92%) and the lowest for bone (75%). The classification performance of CNN is displayed as a confusion matrix in Table 2.

3.2.2. Independent validation set

The panel tissue which performed as the validation set consisted of samples from porcine skeletal muscle ($n = 36$), adipose tissue ($n = 22$), normal breast tissue ($n = 15$), bone ($n = 70$), and liver ($n = 42$). The results are presented in Table 1. We reached the highest accuracy again with CNN (82%) of which the results are visualized in Fig. 4. The specificity for tissue identification ranged between 86% (skeletal muscle) and 100% (adipose tissue and liver). The highest sensitivity (93%) was reached for bone tissue and the lowest sensitivity for adipose tissue (68%) and breast tissue (0%).

3.3. Breast cancer specimens

The utility of iATLAS was further demonstrated with human breast cancer specimens. We performed analyses according to 1) the macroscopic annotation of the samples from photographs and 2) the microscopic annotation of samples from corresponding histology. It should be noted that 10-fold CV is prone to overly optimistic results as the training and test sets are obtained from the same tissue matrices. The classification models can thus learn matrix-specific features which may not generalize to all tissue specimens.

We reached a classification accuracy of 94%, specificity of 94%, and sensitivity of 93% with the macroscopically annotated data from three breast cancer specimens. To visualize the results, measurements

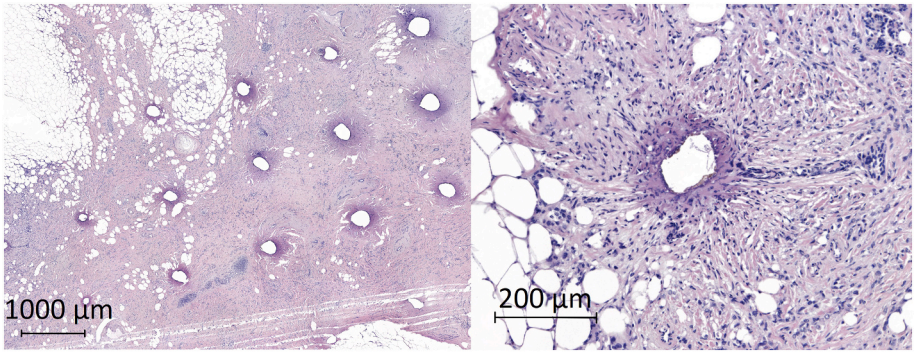

Fig. 2. Histopathological images portraying the dimensions of the measurement points.

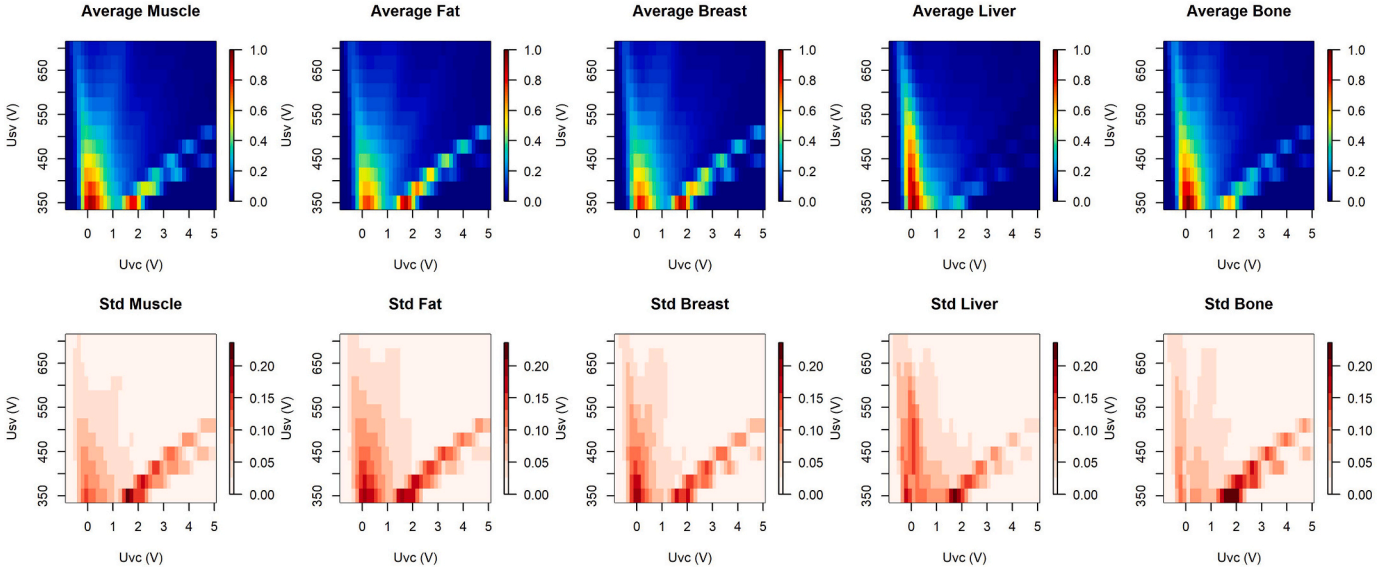

Fig. 3. Averaged dispersion plots of the porcine tissues and corresponding standard deviations across the tissue-wise dispersions.

Table 1
The classification results achieved with shrinkage linear discriminant analysis (sLDA), support vector machine (SVM) with linear and radial kernel, and convolutional neural network (CNN) using the porcine dataset. The classification accuracy, sensitivity and specificity presented for both the leave-one-matrix-out cross-validation (CV) and the independent validation set, respectively.

			Leave-one-matrix-out CV		Independent validation set	
Model	Accuracy	Tissue	Sensitivity (%)	Specificity (%)	Sensitivity (%)	Specificity (%)
sLDA	79.8%; 70.8%	Muscle	80.7	96.6	75.0	81.2
		Fat	84.8	90.0	40.9	97.5
		Breast	62.4	96.4	20.0	99.4
		Liver	75.4	100.0	90.5	99.3
		Bone	76.9	89.0	77.1	82.6
SVM[a]	79.1%; 74.1%	Muscle	79.2	93.9	61.1	92.0
		Fat	87.2	90.6	40.9	98.8
		Breast	69.4	95.6	0.0	100.0
		Liver	83.0	99.9	100.0	97.7
		Bone	65.4	92.1	91.4	73.0
SVM[b]	79.0%; 75.2%	Muscle	81.8	93.7	69.4	92.0
		Fat	88.9	91.0	45.5	100.0
		Breast	61.2	96.7	6.7	98.8
		Liver	76.5	99.8	100.0	94.1
		Bone	63.1	90.7	87.1	79.1
CNN	86.4%; 81.6%	Muscle	89.7	96.9	91.7	85.6
		Fat	92.0	94.2	68.2	100.0
		Breast	77.5	95.2	0.0	99.4
		Liver	81.4	99.9	90.5	100.0
		Bone	75.4	96.0	92.9	89.6

[a] Linear kernel.
[b] Radial kernel.

Table 2
A confusion matrix which presents the leave-one-matrix-out cross-validation (CV) classification results of each tissue type with the convolutional neural network (CNN) model. The tissue types as predicted by the CNN model are presented vertically and the true tissue types horizontally. The CNN classification accuracy was 86%.

	True class (n)				
Predicted class (n)	Muscle	Fat	Breast	Liver	Bone
Muscle	924	37	20	6	15
Fat	42	1223	16	0	72
Breast	42	39	200	0	79
Liver	1	0	0	215	1
Bone	21	30	22	43	513

annotated as uncertain were also classified with the radial SVM model. A visual presentation of the results is presented in Fig. 5.

The classification model for the microscopically annotated data was constructed with samples from two breast cancer specimens. Histologically both samples were of lobular carcinoma. We reached a classification accuracy of 84%, specificity of 88%, and sensitivity of 77% for the first cancer specimen. For the second specimen, the classification accuracy was 72% and specificity 88%, but the sensitivity only 24%. A visual presentation of the results is presented in Fig. 6.

4. Discussion

The performance of a DMS sensor coupled with a laser evaporation unit was stable in the daily measurement series. We achieved a high discrimination rate in porcine tissue classification with CNN in both the matrix-wise CV dataset (86%) and independent validation dataset (82%). We were also able to demonstrate tissue imaging of breast cancer with DMS. The inherent advantage of DMS is its convenience. The samples require minimal preparation prior to analysis and the sampling is automated. DMS technology is robust, and the costs associated with its maintenance are low.

Laser ablation of animal tissues and human colon carcinoma was first presented in 2011. Laser desorption ionization-mass spectrometry (LDI-MS) utilizing a CO_2 laser obtained considerably different spectra of various tissue types, while the subject-to-subject reproducibility of identical tissues was good (Sächfer et al., 2011). The study reported no classification accuracies due to its preliminary nature, but the results support our study design and the utility of CO_2 laser sampling in tissue identification. Genangeli et al. studied tissue identification with Rapid evaporative ionization mass spectrometry (REIMS) in animal tissues with a focus on comparing diathermic and laser sampling. They assessed whether data obtained from either of these methods could be employed to classify the data generated with the other handpiece. They reached a classification accuracy of 87% with a peak list based PVA/LDA model when the diathermy knife data were used to classify the data acquired with laser (Genangeli et al., 2019). Although the study design differed from ours, the results are comparable to our independent validation set results. Our classification accuracy of 82% appears comparable to their highest achieved accuracy and superior to their result concerning all tissue types. However, their model was trained to identify a wider range of tissues. These results emphasize the challenges in creating classification models for several tissue types with external validation datasets as the results consistently fall behind the generally reported leave-one-patient-out CV results (Balog et al., 2013; St John et al., 2017; Zhang et al., 2017).

Emerging MS technologies for breast cancer identification provide a context to our work. The "intelligent knife" (iKnife) aims to real-time intraoperative breast carcinoma detection with REIMS from surgical smoke released during electrosurgical dissection. This system provided a sensitivity of 91% and specificity of 99% with 260 breast specimens using LDA and leave-one-patient-out CV (St John et al., 2017). A major advantage of our method compared to the iKnife is the low penetration depth of laser sampling, allowing analysis even when the biological material is limited. A more recent method called the "MasSpec Pen"

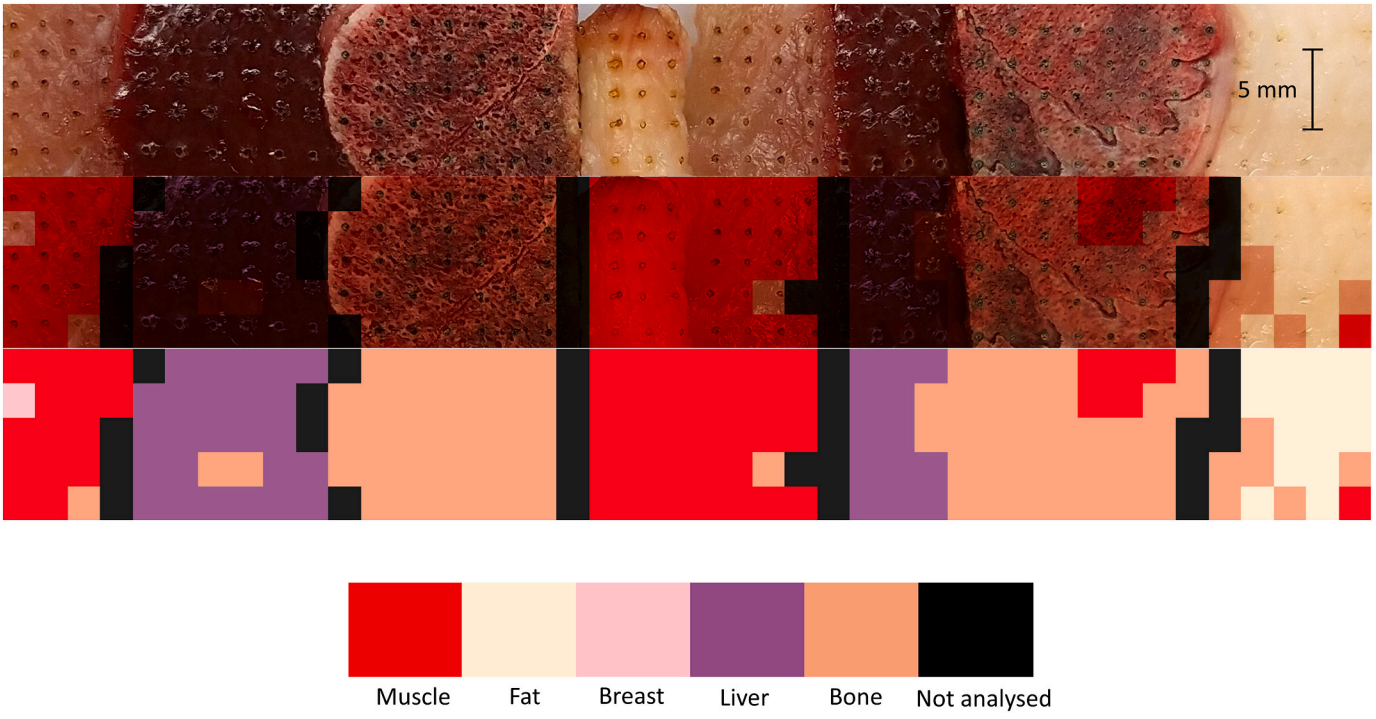

Fig. 4. A visualization of the classification results achieved with the independent validation set. The classification model was constructed with convolutional neural networks (CNNs). Uppermost the panel tissue specimen after sampling. The order of tissues in the uppermost image: skeletal muscle; liver; bone; normal breast tissue; skeletal muscle; liver; bone; and adipose tissue. In the middle an overlapping image of the panel tissue and the classification results. Below solely the classification matrix. The colour bar represents tissue types according to the CNN classification results. The classification accuracy was 82%.

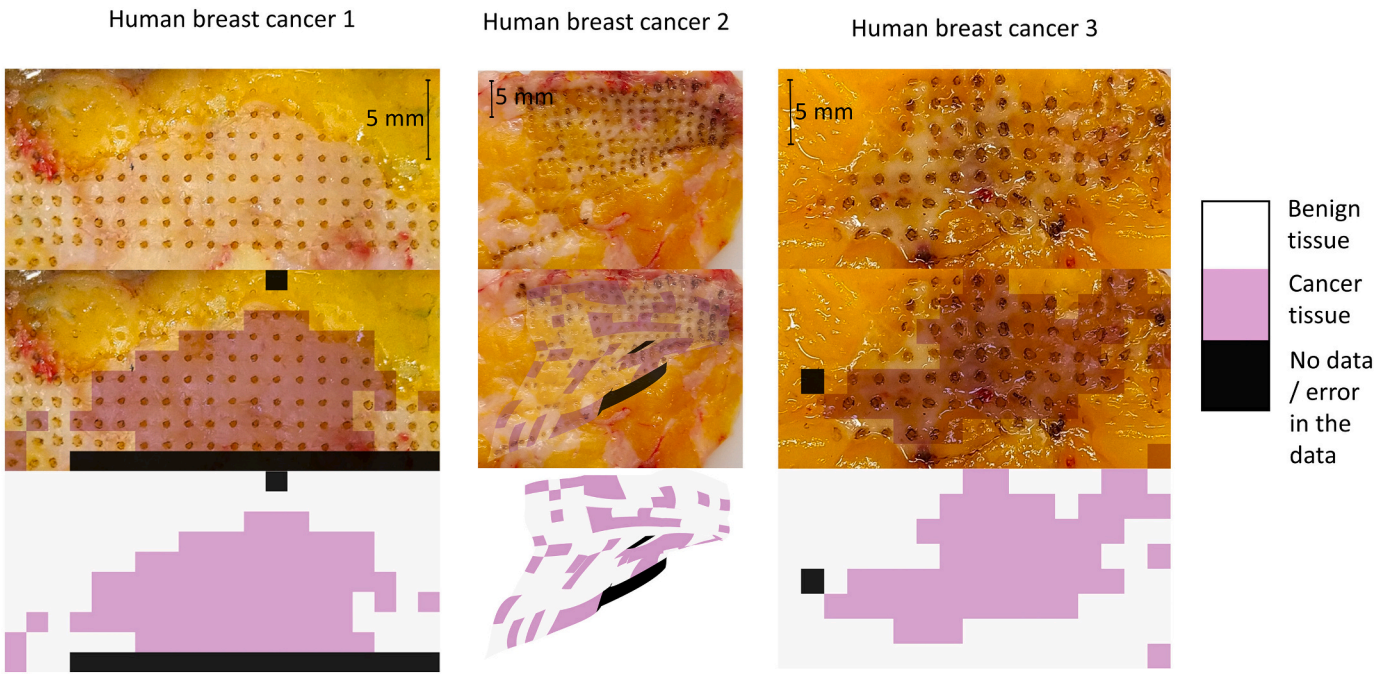

Fig. 5. A visualization of the classification results achieved with the macroscopically annotated breast cancer samples. The applied classification model was support vector machine (SVM) with radial kernel.

utilizes a handheld probe which delivers a water droplet to a tissue surface and enables the extraction of biomolecules without damaging the sample. The analysis of several benign and malignant tissues including forty-five breast tissue measurements achieved breast cancer prediction with 88% sensitivity, 100% specificity, and 96% overall accuracy with Lasso method and leave-one-patient-out CV (Zhang et al., 2017). The probe tip of the MasSpec Pen needs to be washed or removed after each use which impairs its usability in comparison to laser sampling. Desorption Electrospray Ionization-MSI (DESI-MSI) has been showcased in breast cancer imaging. The method enabled the spatial profiling of tissue sections and achieved an overall classification accuracy of 88%, specificity of 90%, and sensitivity of 92%. The analytical process described in the publication was however laborious as all biopsies were first prepared as frozen tissue sections and then subjected to DESI-MSI (Guenther et al., 2015). The performance of MS-based systems surpasses ours, but the inherent advantage of iATLAS is the robustness of the DMS technology. The samples require minimal preparation, system maintenance costs are low, and profuse data pre-processing is not mandated strengthening its clinical suitability.

Other studies on human tissue imaging have focused on liver metastases and colorectal cancer. Veselkov et al. analyzed freshly frozen colorectal cancer samples that were cryo-sectioned and subjected to DESI-MSI. The performance exceeded 98% in the classification of cancerous and benign tissues (Veselkov et al., 2014). Mirnezami et al. studied the differences in lipid biochemistry of cancerous and healthy colorectal tissue and tumor-adjacent tissue with Matrix assisted laser desorption/ionization-MSI (MALDI-MSI). They showed that cancerous and tumor-adjacent tissues harbor characteristic phospholipid signatures but did not report classification accuracies limiting the comparison of results to ours in this respect (Mirnezami et al., 2014). While DESI and MALDI yield accurate results, the associated hardware costs and maintenance requirements are ample, and the methods are time-consuming due to their complex sampling, sectioning, data pre-processing, and imaging processes. MS-based systems are also large as opposed to iATLAS. To suit clinical practice, the system should be practical and operate without significant delay. iATLAS reaches spatially comprehensive but less accurate analysis with minimal sample preparation compared to MSI techniques. In future, the method could be utilized to direct sampling before the conventional gold standard analysis of fixation and staining.

The achieved classification accuracies in breast cancer imaging are preliminary and a larger follow-up study is necessary to provide reliable sensitivity and specificity numbers for the method. However, we successfully presented an efficient and repeatable process to analyze breast cancer with DMS and to annotate these samples microscopically. We were unable to obtain a corresponding histology for one breast cancer specimen but went on to improve the study protocol. For the microscopic annotations, the achieved sensitivities differed significantly between the two specimens. The histologic features of the lobular carcinomas were also distinct (Fig. 5). The invasive carcinoma was unifocal in the first sample. In the second sample, the carcinoma cells loosely dispersed throughout the fibrous stroma in a discohesive morphologic pattern. The scattering of malignant samples among benign samples can result in a low sensitivity due to the varying cell density and mixing of consecutive samples due to carry-over. Despite these limitations, the results remain encouraging and support future studies as we achieved a high classification accuracy with the data accumulated from animal tissues and demonstrated iATLAS in breast cancer imaging.

The limitations of the study included system malfunctions, shift in measurement parameters, and restrictions of the classification models. The system function complications of iATLAS were due to the faulty production of dispersion plots. These resulted from the prototype nature of the system and have later been fixed with software updates. Altogether, these malfunctions were seldom ($n = 67$), and the overall system performance was stable. The ENVI-AMC® DMS is a first-generation prototype of which the analytical performance can be improved by developing its components. Our future goal is to utilize a next-generation DMS sensor to enhance classification. We identified a dynamic drift in measurements likely resulting from a drift in the hardware or environmental factors. This was addressed by normalizing the measurement intensities. Complex classification models improve with an increased sample size. The majority of the porcine tissue samples were ample and gathered from multiple animals. However, the number of bone and normal breast tissue measurements were fewer, which likely influenced the classification results negatively. In matrix-wise tissue

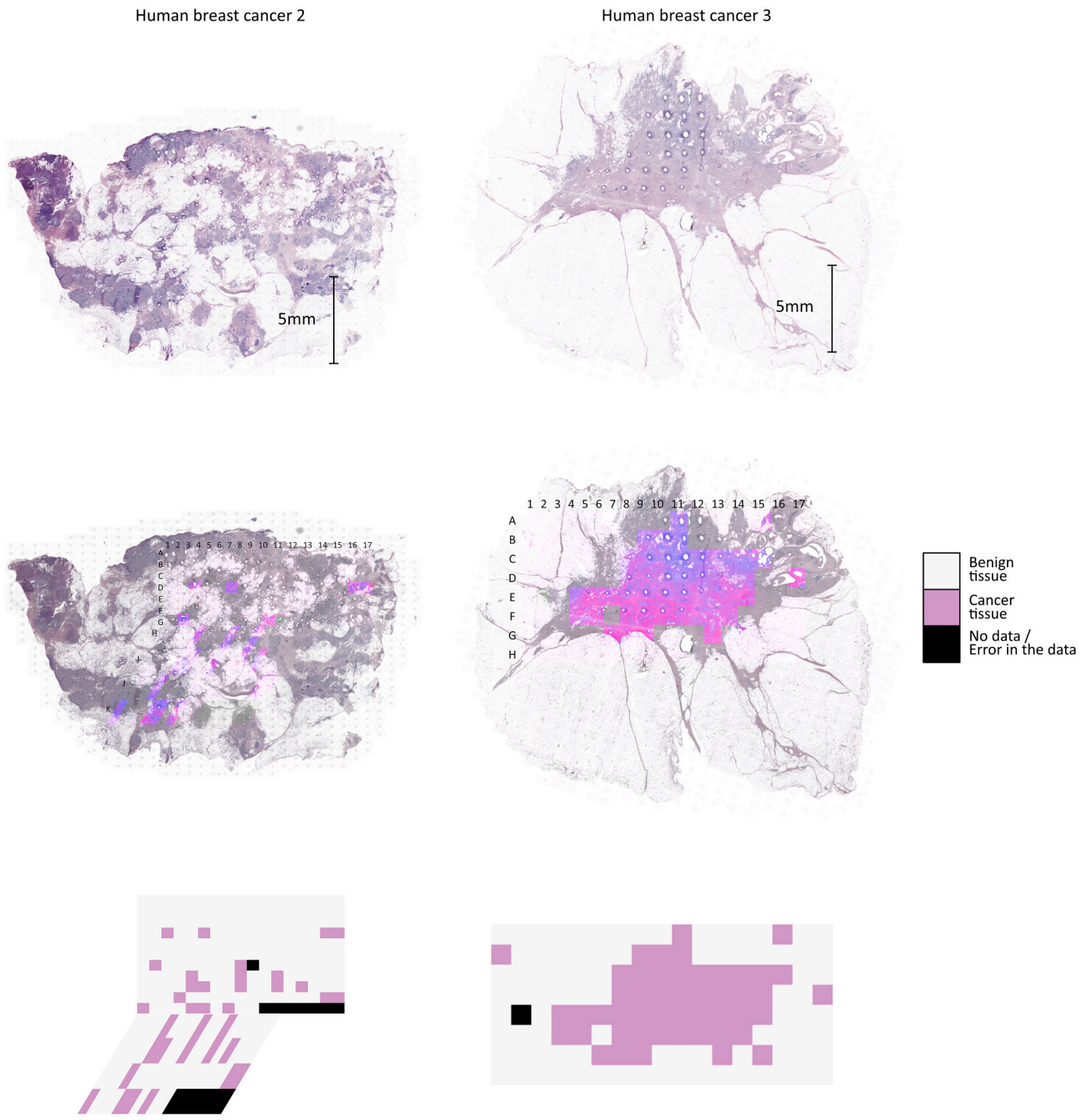

Fig. 6. A visualization of the classification results achieved with the microscopically annotated breast cancer samples. The applied classification model was support vector machine (SVM) with radial kernel.

identification, bone samples were categorized most often falsely as adipose tissue or breast tissue whereas all breast samples in the independent validation set were classified as skeletal muscle. In matrix-wise tissue identification, we analyzed the breast samples as a part of a larger specimen. For the independent validation set, we gathered samples that mainly comprised breast gland parenchyma after careful inspection and palpation. The validation set should consist of similar samples as the training set to ensure representative results. The differences in datasets likely contributed to the compromised sensitivity for breast tissue identification in the independent validation set analysis. Closely measured samples have similar qualities due to alike tissue features and carry-over, which can lead to overfitting with traditional n-fold CV. We explored the overoptimization of 10-fold CV in practice with the porcine classification models, and all models reached an accuracy exceeding 95% with 10-fold CV. Therefore, we applied CV over the matrices instead of samples to reduce this bias. As priorly discussed, CV over the matrices was not applicable to the breast cancer samples due to sample size which limits the reliability of results and should be factored in their interpretation.

5. Conclusions

The differentiation of tissues from surgical smoke created with a laser can be achieved with a first-generation DMS device in a laboratory setting. We showed that the DMS spectra of identical tissues correlate strongly regardless of the time of analysis and reached good classification results in the porcine classification models. Our results also suggest that non-linear classification methods exceed the performance of linear methods. Especially CNNs have a high potential in the analysis of DMS data. In addition, we demonstrated the DMS analysis of human breast cancer specimens successfully. In future, pre-mapping of breast specimens before their pathological gross examination could indicate neoplastic areas to the pathologist and enable focused sampling from areas that likely contain malignant tissue. This could allow for pathological examination with a reduced number of analyzed sections without compromising diagnostic accuracy.

Funding

Maiju Lepomäki declares funding from the Doctoral School of Tampere University, The Finnish Medical Foundation [grant numbers 2167, 4038], and Cancer Foundation of Finland. Anton Kontunen declares funding from the Doctoral School of Tampere University, The Finnish Foundation for Technology Promotion [grant number 7671], and Emil Aaltonen Foundation [grant number 210073K]. This study has received funding from the ATTRACT project funded by the European Commission from the Horizon 2020 research and innovation programme [grant agreement 777222]. This study was also financially supported by Competitive State Research Financing of the Expert Responsibility Area of Tampere University Hospital and Pirkanmaa Hospital District [grant numbers 9AA057, 9x040, 9v044, 9T044, 9U042, 9s045, 150618, 151B03]; Competitive funding to strengthen university research profiles funded by the Academy of Finland [decision number 292477]; and from the Tampere Tuberculosis Foundation. The study sponsors did not have any involvement in the study design; collection, analysis and interpretation of data; the writing of the manuscript; or the decision to submit the manuscript for publication.

Data statement

The datasets used and analyzed during the current study are available from the corresponding author on reasonable request.

CRediT authorship contribution statement

Maiju Lepomäki: Conceptualization, Methodology, Investigation, Resources, Writing – original draft, Writing – review & editing. **Anna Anttalainen:** Conceptualization, Methodology, Software, Validation, Formal analysis, Data curation, Writing – original draft, Writing – review & editing, Visualization. **Artturi Vuorinen:** Methodology, Software, Investigation, Resources, Writing – review & editing, Visualization. **Teemu Tolonen:** Methodology, Investigation, Resources, Writing – review & editing. **Anton Kontunen:** Methodology, Software, Resources, Writing – review & editing. **Markus Karjalainen:** Methodology, Software, Resources, Writing – review & editing. **Antti Vehkaoja:** Conceptualization, Methodology, Resources, Writing – review & editing, Supervision, Project administration, Funding acquisition. **Antti Roine:** Conceptualization, Methodology, Resources, Writing – original draft, Writing – review & editing, Supervision, Project administration, Funding acquisition. **Niku Oksala:** Conceptualization, Methodology, Resources, Writing – review & editing, Supervision, Project administration, Funding acquisition.

Declaration of Competing Interest

Antti Roine, Niku Oksala, Anton Kontunen and Markus Karjalainen are shareholders and employees of Olfactomics Ltd., a medical device company that develops novel technology for intraoperative surgical margin assessment. Anna Anttalainen is an employee of Olfactomics Ltd. The remaining authors declare that there are no conflicts of interest.

Acknowledgements

We thank the personnel of Paija slaughterhouse (Paijan tilateurastamo, Urjala, Finland) and the staff of Fimlab Laboratories' pathology laboratory for their assistance in this study.

Appendix A. Supplementary data

Supplementary data to this article can be found online at https://doi.org/10.1016/j.yexmp.2022.104759.

References

Abadi, M., Agarwal, A., Barham, P., Brevdo, E., Chen, Z., Citro, C., Corrado, G.S., Davis, A., Dean, J., Devin, M., Ghemawat, S., Goodfellow, I., Harp, A., Irving, G., Isard, M., Jia, Y., Jozefowicz, R., Kaiser, L., Kudlur, M., Levenberg, J., Mané, D., Monga, R., Moore, S., Murray, D., Olah, C., Schuster, M., Shlens, J., Steiner, B., Sutskever, I., Talwar, K., Tucker, P., Vanhoucke, V., Vasudevan, V., Viégas, F., Vinyals, O., Warden, P., Wattenberg, M., Wicke, M., Yu, Y., Zheng, X., 2016. TensorFlow: large-scale machine learning on heterogeneous distributed systems. Software. https://doi.org/10.5281/zenodo.4724125 available from. tensorflow.org.

Ahdesmäki, M., Strimmer, K., 2010. Feature selection in omics prediction problems using cat scores and false nondiscovery rate control. Ann. Appl. Stat. 4, 503–519. https://doi.org/10.1214/09-AOAS277.

Ahdesmaki, M., Zuber, V., Gibb, S., Strimmer, K., 2015. SDA: shrinkage discriminant analysis and CAT score variable selection. R package version 1.3.7. https://CRAN.R-project.org/package=sda.

Allaire, J., Chollet, F., 2019. Keras: R Interface to 'Keras'. R package version 2.2.5.0. https://cloud.r-project.org/package=keras.

Anttalainen, A., Mäkelä, M., Kumpulainen, P., Vehkaoja, A., Anttalainen, O., Oksala, N., Roine, A., 2021. Predicting lecithin concentration from differential mobility spectrometry measurements with linear regression models and neural networks. Talanta 225, 121926. https://doi.org/10.1016/j.talanta.2020.121926.

Balog, J., Sasi-Szabo, L., Kinross, J., Lewis, M.R., Muirhead, L.J., Veselkov, K., Mirnezami, R., Dezso, B., Damjanovich, L., Darzi, A., Nicholson, J.K., Takats, Z., 2013. Intraoperative tissue identification using rapid evaporative ionization mass spectrometry. Sci. Transl. Med. 5, 194ra93. https://doi.org/10.1126/scitranslmed.3005623.

Cardoso, F., Kyriakides, S., Ohno, S., Penault-Llorca, F., Poortmans, P., Rubio, I.T., Zackrisson, S., Senkus, E., 2019. Early breast cancer: ESMO clinical practice guidelines for diagnosis, treatment and follow-up. Ann. Oncol. 30, 1194–1220. https://doi.org/10.1093/annonc/mdz189.

Corna, K.C., Windhama, M.A., Rafata, M., 2020. Lipids in the tumor microenvironment: from cancer progression to treatment. Prog. Lipid Res. 80, 101055 https://doi.org/10.1016/j.plipres.2020.101055.

Cortes, C., Vapnik, V., 1995. Support-vector networks. Mach. Learn. 20, 273–297. https://doi.org/10.1007/BF00994018.

Covington, J.A., van der Schee, M.P., Edge, A.S.L., Boyle, B., Savage, R.S., Arasaradnam, R.P., 2015. The application of FAIMS gas analysis in medical diagnostics. Analyst 140, 6775–6781. https://doi.org/10.1039/C5AN00868A.

Cumeras, R., Figueras, E., Davis, C.E., Baumbach, J.I., Gràcia, I., 2015. Review on ion mobility spectrometry. Part 1: current instrumentation. Analyst 14. https://doi.org/10.1039/C4AN01100G, 1376–139.

Genangeli, M., Heeren, R., Siegel, T., 2019. Tissue classification by rapid evaporative ionization mass spectrometry (REIMS): comparison between a diathermic knife and CO_2 laser sampling on classification performance. Anal. Bioanal. Chem. 411, 7943–7955. https://doi.org/10.1007/s00216-019-02148-8.

Golf, O., Strittmatter, N., Karancsi, T., Pringle, S.D., Speller, A.V.M., Mroz, A., Kinross, J. M., Abbassi-Ghadi, N., Jones, E.A., Takats, Z., 2015. Rapid evaporative ionization mass spectrometry imaging platform for direct mapping from bulk tissue and bacterial growth media. Anal. Chem. 87, 2527–2534. https://doi.org/10.1021/ac5046752.

Goodfellow, I., Bengio, Y., Courville, A., 2016. Deep Learning. The MIT Press. http://www.deeplearningbook.org.

Guenther, S., Muirhead, L.J., Speller, A.V.M., Golf, O., Strittmatter, N., Ramakrishnan, R., Goldin, R.D., Jones, E., Veselkov, K., Nicholson, J., Darzi, A., Takats, Z., 2019. Spatially resolved metabolic phenotyping of breast Cancer by desorption electrospray ionization mass spectrometry. Cancer Res. 75, 1828–1837. https://doi.org/10.1158/0008-5472.CAN-14-2258.

Haapala, I., Karjalainen, M., Kontunen, A., Vehkaoja, A., Nordfors, K., Haapasalo, H., Haapasalo, J., Oksala, N., Roine, A., 2019. Identifying brain tumors by differential mobility spectrometry analysis of diathermy smoke. J. Neurosurg. 133, 100–106. https://doi.org/10.3171/2019.3.JNS19274.

Hancock, S.E., Poad, B.L.J., Willcox, M.D.P., Blanksby, S.J., Mitchell, T.W., 2019. Analytical separations for lipids in complex, nonpolar lipidomes using differential

mobility spectrometry. J. Lipid Res. 60, 1968–1978. https://doi.org/10.1194/jlr.D094854.
Institute of Biosciences and Medical Technology, 2017. Kudoslaki ja siihen liittyvät asetukset. http://cofa.uta.fi/med/naytelait/lait_kudos.html (accessed 11 December, 2020).
Kontunen, A., Karjalainen, M., Lekkala, J., Roine, A., Oksala, N., 2018. Tissue identification in a porcine model by differential ion mobility spectrometry analysis of surgical smoke. Ann. Biomed. Eng. 46, 1091–1100. https://doi.org/10.1007/s10439-018-2035-5.
Kontunen, A., Tuominen, J., Karjalainen, M., Anttalainen, O., Tolonen, T., Kumpulainen, P., Lepomäki, M., Vehkaoja, A., Oksala, N., Roine, A., 2020. Differential mobility spectrometry imaging for pathological applications. Exp. Mol. Pathol. 117, 104526 https://doi.org/10.1016/j.yexmp.2020.104526.
Liberti, M.V., Locasale, J.W., 2016. The Warburg effect: how does it benefit Cancer cells? Trends Biochem. Sci. 41, 211–218. https://doi.org/10.1016/j.tibs.2015.12.001.
Lovrics, P.J., Cornacchi, S.D., Farrokhyar, F., Garnett, A., Chen, V., Franic, S., Simunovic, M., 2009. The relationship between surgical factors and margin status after breast-conservation surgery for early stage breast cancer. Am. J. Surg. 197, 740–746. https://doi.org/10.1016/j.amjsurg.2008.03.007.
Maloney, B.W., McClatchy, D.M., Pogue, B.W., Paulsen, K.D., Wells, W.A., Barth, R.J., 2018. Review of methods for intraoperative margin detection for breast conserving surgery. J. Biomed. Opt. 23, 100901 https://doi.org/10.1117/1.JBO.23.10.100901.
Meyer, D., Dimitriadou, E., Hornik, K., Weingessel, A., Leisch, F., 2019. e1071: Misc functions of the Department of Statistics, probability theory group (formerly: E1071), TU Wien. R package version 1.7.3. https://rdrr.io/rforge/e1071/.
Mirnezami, R., Spagou, K., Vorkas, P.A., Lewis, M.R., Kinross, J., Want, E., Shion, H., Goldin, R.D., Darzi, A., Takats, Z., Holmes, E., Cloarec, O., Nicholson, J.K., 2014. Chemical mapping of the colorectal cancer microenvironment via MALDI imaging mass spectrometry (MALDI-MSI) reveals novel cancer-associated field effects. Mol. Oncol. 8, 39–49. https://doi.org/10.1016/j.molonc.2013.08.010.
Morrow, M., 2009. Breast conservation and negative margins: how much is enough? Breast 18, 84. https://doi.org/10.1016/S0960-9776(09)70279-6.
Nunez, A., Jones, V., Schulz-Costello, K., Schmolze, D., 2020. Accuracy of gross intraoperative margin assessment for breast cancer: experience since the SSO-ASTRO margin consensus guidelines. Sci. Rep. 10, 17344. https://doi.org/10.1038/s41598-020-74373-6.
Ogrinc, N., Saudemont, P., Balog, J., Robin, Y., Gimeno, J., Pascal, Q., Tierny, D., Takats, Z., Salzet, M., Fournier, I., 2019. Water-assisted laser desorption/ionization mass spectrometry for minimally invasive in vivo and real-time surface analysis using SpiderMass. Nat. Protoc. 14, 3162–3182. https://doi.org/10.1038/s41596-019-0217-8.
R Core Team, 2018. A Language and Environment for Statistical Computing. R Foundation for Statistical Computing, Vienna, Austria. https://www.R-project.org/.
R Core Team, 2019. A Language and Environment for Statistical Computing. R Foundation for Statistical Computing, Vienna, Austria. https://www.R-project.org/.
Sächfer, K., Szaniszló, T., Günther, S., Balog, J., Dénes, J., Keseru, M., Dezso, B., Tóth, M., Spengler, B., Takáts, Z., 2011. In situ, real-time identification of biological tissues by ultraviolet and infrared laser desorption ionization mass spectrometry. Anal. Chem. 83, 1632. https://doi.org/10.1021/ac102613m.
Senkus, E., Kyriakides, S., Ohno, S., Penault-Llorca, F., Poortmans, P., Rutgers, E., Zackrisson, S., Cardoso, F., 2015. Primary breast cancer: ESMO clinical practice guidelines for diagnosis, treatment and follow-up †. Ann. Oncol. 26, v8–v30. https://doi.org/10.1093/annonc/mdv298.
Shvartsburg, A.A., Isaac, G., Leveque, N., Smith, R.D., Metz, T.O., 2011. Separation and classification of lipids using differential ion mobility spectrometry. J. Am. Soc. Mass Spectrom. 22, 1146–1155. https://doi.org/10.1007/s13361-011-0114-z.
St John, E.R., Balog, J., McKenzie, J.S., Rossi, M., Covington, A., Muirhead, L., Bodai, Z., Rosini, F., Speller, A.V.M., Shousha, S., Ramakrishnan, R., Darzi, A., Takats, Z., Leff, D.R., 2017. Rapid evaporative ionisation mass spectrometry of electrosurgical vapours for the identification of breast pathology: towards an intelligent knife for breast cancer surgery. Breast Cancer Res. 19, 59. https://doi.org/10.1186/s13058-017-0845-2.
Sutinen, M., Kontunen, A., Karjalainen, M., Kiiski, J., Hannus, J., Tolonen, T., Roine, A., Oksala, N., 2019. Identification of breast tumors from diathermy smoke by differential ion mobility spectrometry. Eur. J. Surg. Oncol. 45, 141–146. https://doi.org/10.1016/j.ejso.2018.09.005.
van Leeuwen, M.T., Falster, M.O., Vajdic, C.M., Crowe, P.J., Lujic, S., Klaes, E., Jorm, L., Sedrakyan, A., 2018. Reoperation after breast-conserving surgery for cancer in Australia: statewide cohort study of linked hospital data. BMJ Open 8, e020858. https://doi.org/10.1136/bmjopen-2017-020858.
Vaupel, P., Schmidberger, H., Mayer, A., 2019. The Warburg effect: essential part of metabolic reprogramming and central contributor to cancer progression. Int. J. Radiat. Biol. 95, 912–919. https://doi.org/10.1080/09553002.2019.1589653.
Veselkov, K.A., Mirnezami, R., Strittmatter, N., Goldin, R.D., Kinross, J., Abigail, V.M.S., Abramov, T., Jones, E.A., Darzi, A., Holmes, E., Nicholson, J.K., Takats, Z., 2014. Chemo-informatic strategy for imaging mass spectrometry-based hyperspectral profiling of lipid signatures in colorectal cancer. PNAS. 111, 1216–1221. https://doi.org/10.1073/pnas.1310524111.
Zhang, J., Rector, J., Lin, J.Q., Young, J.H., Sans, M., Katta, N., Giese, N., Yu, W., Nagi, C., Suliburk, J., Liu, J., Bensussan, A., Dehoog, R.J., Garza, K.Y., Ludolph, B., Sorace, A.G., Syed, A., Zahedivash, A., Milner, T.E., Eberlin, L.S., 2017. Nondestructive tissue analysis for ex vivo and in vivo cancer diagnosis using a handheld mass spectrometry system. Sci. Transl. Med. 9, eaan3968. https://doi.org/10.1126/scitranslmed.aan3968.